

Chapter-3

Study of volcanic tephra deposits in the Andaman region

3.1 Introduction

Cenozoic volcanism has been described throughout the Andaman region including Myanmar in the north to Sumatra-Java in the south (Chhibber, 1934) (Fig. 3.1a). From Myanmar mafic to intermediate type calcalkaline volcanism has been reported (Chhibber, 1934, Mitchell, 1985) while in Sumatra, Java and Sundaland felsic volcanism is predominant (Wakita, 2000; Wakita et al. 1998; Hall 2002, 2009; Van Bemmelen, 1949). This volcanism is related to subduction of the Indian plate under the Eurasian plate and represents the volcanic/magmatic arc since Cretaceous (Curry and Moore, 1974). Pyroclastics and ash derived from these volcanoes have been deposited along with the terrigenous sediments in trench-slope, forearc and back arc basins and many such deposits are currently exposed in the Andaman-Nicobar Islands. Identification and study of these ash beds are likely to reveal a great deal about the volcanism in the region since Cretaceous.

Ash beds found in sediments from the Indian Ocean surrounding continents point to a widespread volcanic activity in the region in the recent past (e.g. Ninkovich et al. 1978; Rose and Chesner 1987; Dehn et al. 1991; Westgate et al, 1998; Pattan et al, 1999; Schulz et al. 1998). However, chronology and geochemistry of these ash deposits suggest that most of them are linked to the last three major eruptions of Toba in Sumatra those happened during the Quaternary (e.g. Pattan et al. 2001 and references therein; Rose and Chesner 1987). In the Andaman region, there have been several reports of ash (pyroclastic) deposits interbedded with forearc sediments of the south Andaman Island, Rutland Island and Havelock Island and are approximately of Eocene through Pliocene in age (e.g., Bandopadhyay, 2005; Pal et al., 2003, 2005, 2010a; Pawde and Ray 1963; Srinivasan 1988; Pal et al., 2002). The source(s) of these ash deposits are not yet known. Andaman Sea, which came into existence during late Miocene to early Pliocene (Khan and Chakraborty, 2005), is also an important site for investigation of records of past volcanism in the region because of its proximity to the

volcanic arc of Banda-Sunda and Andaman subduction zones (Fig. 3.1a). In addition, since the Andaman Sea is a semi-enclosed basin (Kurian et al., 2008), with restricted submarine transport and dispersal, the preservation of volcanic record in the sediments deposited in the basin is likely to be complete, therefore, its marine sedimentary record would be the best proxy of regional volcanism since the opening of the basin in Tertiary.

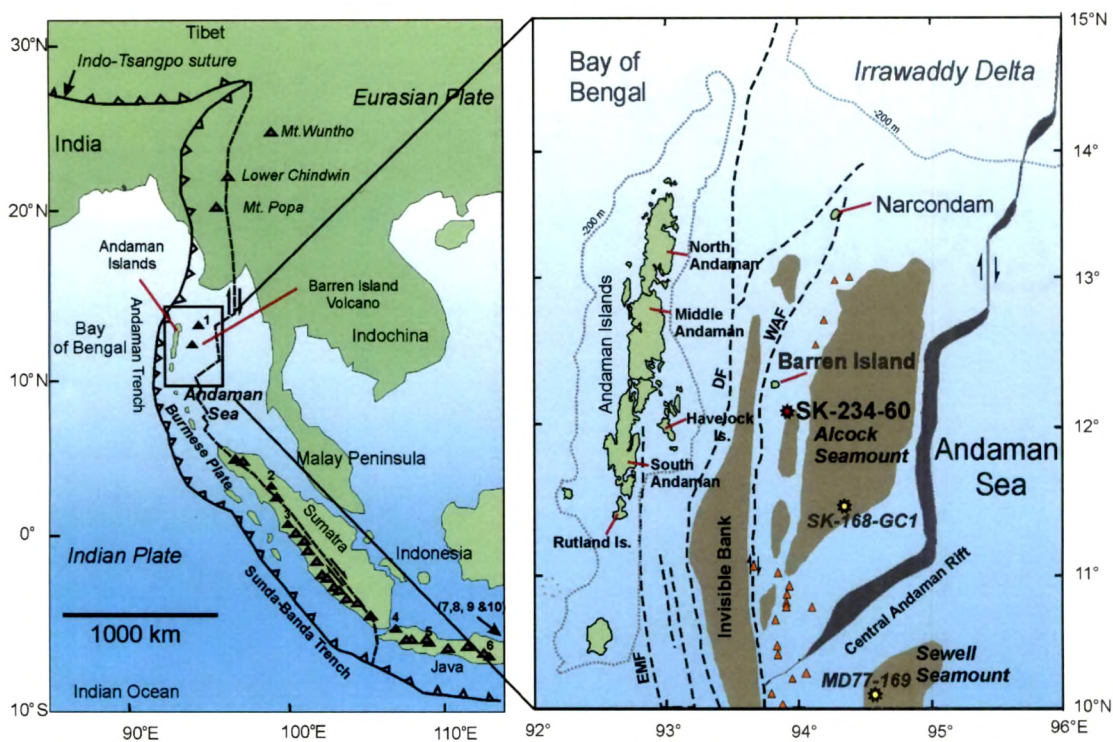


Fig. 3.1: Map of Southeast Asia showing major tectonic features and eruptive centres including the Barren Island Volcano ($N12^{\circ}16'40''$, $E93^{\circ}51'30''$) and other volcanoes of the Indonesian Arc. The numbered volcanoes are (1) Narcondam (2) Toba, (3) Sorimerapi, (4) Krakatoa, (5) Galunggung, (6) Merapi, (7) Rinjani, (8) Tambora, (9) Sangeang Api and (10) Iya Flores. The enlarged portion shows the locations of the deep-sea cores in red and yellow stars, respectively. Core SK-234-60 is from this work while cores MD-77-169 (Colin et al., 1999) and SK 168/GC-1 (Sijinkumar et al, 2010) are other cores studied from nearby locations. The figure also shows Alcock, Sewell and other volcanic seamounts (in triangles) of the Andaman Sea.

3.2 Records of volcanism from the Andaman Islands

The oldest record of volcanism in the Andaman region comes from the Eocene age Namunagarh Grit Formation (Fig. 3.2a), which contains pyroclastics: abundant glass shards, lithic fragments, plagioclase crystals and altered glassy matrix (Bandopadhyay, 2005). On the basis of sedimentary, petrographic and geochemical attributes, these materials are believed to have been derived from explosive arc volcanoes

(Bandopadhyay, 2005). Bandopadhyay (2005) inferred that this deposit was produced as a result of shallow subaqueous or subaerial phreatomagmatic eruption and rapid deposition in deep waters in a forearc setting, as debris flows and turbidites. Several thick sequences of felsic ash (tuff) beds have also been described from the Mio-Pliocene calcareous and non-calcareous sediments of the Archipelago Group of Rutland Island (Pal et al., 2010a), from Hubdaypur and Mile Tilek area of the south Andaman and from Havelock Island of the Ritchie's Archipelago (Pal et al., 2005) (Fig. 3.1b). From these localities, greenish to white and pinkish white facies of the ash beds (tuff) have been reported. These deposits were believed to have been generated by subaerial eruptions, however, evidences suggest that these were transported in subaqueous condition and deposited by high concentration turbidity currents (Pal et al., 2005, 2010a).



Fig. 3.2: Field photographs showing (a) pyroclastic sandstones of Namunagarh Grit Formation at Namunagarh (b) Felsic Tuff in the Archipelago Group at Mile Tilek.

Several hypotheses have been proposed by earlier workers to explain the source(s) of these ash beds. As the occurrences of these ash beds were predominantly restricted to the eastern part of the main islands, Bandopadhyay, (2005) speculated that the inner arc volcanoes located on the western margin of the Burma–Thai–Malaya Peninsula, which were predominantly felsic in nature, were the sources of these deposits. Ocean-continent type subduction must be occurring at that time to produce felsic magmas, however, at present there exists no evidence for such an arc on the continental plate east of the Andaman Sea. The inner volcanic arc located east of the Andaman Islands seems to be quite young and probably came into existence only after the opening of the Andaman Sea in the Late Miocene. Pal et al. (2010a) suggested that the early to middle Miocene felsic volcanic activity of Sumatra was a major source of dacitic and trachytic type ash beds found in the Andamans and that these ashes were transported to long distances in submarine conditions. Hall (2002, 2009) have also reported felsic volcanism of middle to late Miocene age from the Sundaland shelf. It is not clear as to why Myanmar volcanic sources have been neglected by earlier studies, however, in spite of the facts that the sedimentary formations of Andaman Islands received much of its sediments from the north (Pal et al., 2003). Locating the exact sources of volcanogenic sediments would require more clues from geochemical and isotopic studies and a clear understanding of the paleogeographic configuration of the various tectonic blocks in this region.

3.3 Records of volcanism from the Andaman Sea

Despite the fact that the Andaman Sea was created in late Miocene and that it lies east and north of the Andaman-Indonesia volcanic arc, not many workers have reported ash layers in sediment cores. In one such study Colin et al. (1999) reported an ash layer in a sediment core (MD77-169) from the Sewell Seamount (Fig. 3.1b), and suspected it to represent the youngest eruption of the famous Toba volcano of Indonesia. The N-S trending inner arc of the Andaman subduction zone is located on the western flank of the Andaman Sea and it contains two subaerial volcanoes, the active Barren Island Volcano and the dormant Narcondam (Fig. 3.1b). There exist several other prominent underwater mountains possibly of volcanic origin (Fig. 3.1b) (Curry, 2005, Kamesh Raju et al., 2012). Barren Island is the northernmost active center of the volcanic arc and acts as a link between the active volcanic arc of Java-Sumatra and the extinct or

dormant volcanoes of Myanmar (e.g., Mt. Popa, fissure vents of Singu Plateau) (Stephenson and Marshall, 1984) (Fig. 3.1a). Narcondam, located 135 km north-northeast of the Barren Island Volcano, is another volcano, believed to have come into existence during Late Pliocene to Pleistocene (Streck et al., 2011). The composition of lava and ash from the Barren Island Volcano is basaltic to basaltic andesite, whereas of Narcondam varies from basaltic to rhyolitic (Sheth et al., 2009a; Pal et al., 2007b).

Most part of these volcanoes have evolved below sea level, which suggests that their eruptive history is older than the timing of their emergence above the sea surface. The subaerially exposed parts of these volcanoes consist of volcanoclastic deposits and lava flows of unknown age. Inaccessible terrain, thick forest, lack of old exposures and unavailability of suitable samples for dating and geochemical studies have restricted extensive studies to be carried out on these volcanoes. Initial attempts to date the lavas from Barren Island and Narcondam have had limited success (Banerjee, 2010; Streck et al., 2011). Dates from Narcondam, although have very large errors, suggest that the activity of the volcano goes back in time to at least ~700 ka and the youngest eruption occurred sometime during the Holocene (Streck et al., 2011). Dating of these volcanic features and their eruptive products is essential in understanding the evolution of the inner arc in the Andaman region.

Deep marine sediment record have often been used in establishing history of large scale volcanism in a region by studying ash layers preserved in them (e.g., Carel et al, 2011; Fretzdorff and Smellie, 2002). Identifying ash beds/layers preserved in ocean basins and linking them to nearby or distant volcanoes through isotope/geochemical fingerprinting can reveal a great deal of information about the volcanic history of the surrounding region and in a few cases about mega volcanic events of global importance. Detailed mineralogical and geochemical studies can also help in understanding the nature, source, eruptive and depositional history of these volcanogenic sequences both in time and space. In an effort to build a history of volcanism in the Andaman region since the opening of the Andaman Sea, we have studied ash layers from a marine sediment core (SK-234, Fig. 3.1b). The results of this study are discussed in following paragraphs.

3.4 Study of ash layers in a sediment core from the Andaman Sea

3.4.1 Description of ash layers and geochronology

The four meter gravity sediment core (SK-234) collected from location N12°16'40", E93°51'30" (Fig. 3.1b) predominantly contained fine-grained terrigenous sediments and pelagic carbonates. Seven distinct ash layers were identified on the basis of darker color, coarser grain size, and presence of glass shards and magmatic minerals such as pyroxene and plagioclase (confirmed by microscopy and x-ray diffractometry). These ash layers were found to occur below the sea floor at intervals of 53–57 (AL-1), 73–75 (AL-2), 90–94 (AL-3), 109–112 (AL-4), 302–321 (AL-5), 372–377 (AL-6) and 380–387 (AL-7) cm (Fig. 3.3). The grain size of these layers was more than 62 μm and the 302–321 cm layer was the coarsest of all. Apart from the distinct ash layers we also observed dispersed (< 10 % by volume) glass shards and grains of volcanic fragments in the marine sediments (clay/sand/carbonates) at many places in the core. These grains may represent minor ash eruptions of the volcano or reworked ash from any subaerial exposure.

In the core all distinct ash layers were separated from terrigenous sediments and pelagic carbonates by decarbonation and gravity separation, detailed procedure of which is discussed in Chapter-2. For source identification, Sr-Nd isotopic ratio measurements were carried out on aggregate samples of unaltered glass shards, lithic fragments and crystal grains, of each ash layer of the core. These measurements were also carried on the samples of ten ash beds from subaerial exposures of nearby Barren Island Volcano (Fig. 3.1b), and a couple of lava flows from the Narcondam Volcano in order to compare them with those of the ash layers in the core. To determine the chronology of these events planktic foraminifers from sediment layers were picked for AMS radiocarbon dating (Fig. 3.3). Major element contents of glass and lithic fragments were determined by an EPMA to characterize the eruptions and understand the magmatic evolution of the source volcano(es).

The samples for dating were selected in such a way that their depositional ages could be utilized to estimate the ages of the ash layers. The AMS ^{14}C ages obtained for the dated sediment layers in the core are given in Fig. 3.3 with 1σ errors. Progressively increasing ages with depth, of sediments except for the top 20 cm, confirm the core's

undisturbed nature. Using these ages we determined the rates of sedimentation between the nine dated bands (Fig. 3.4). All calculations were based on the assumption that the ages represented the mean depths of the sampled intervals (or bands). In the calculations, each ash layer, irrespective of its thickness was assumed to represent an instantaneous event.

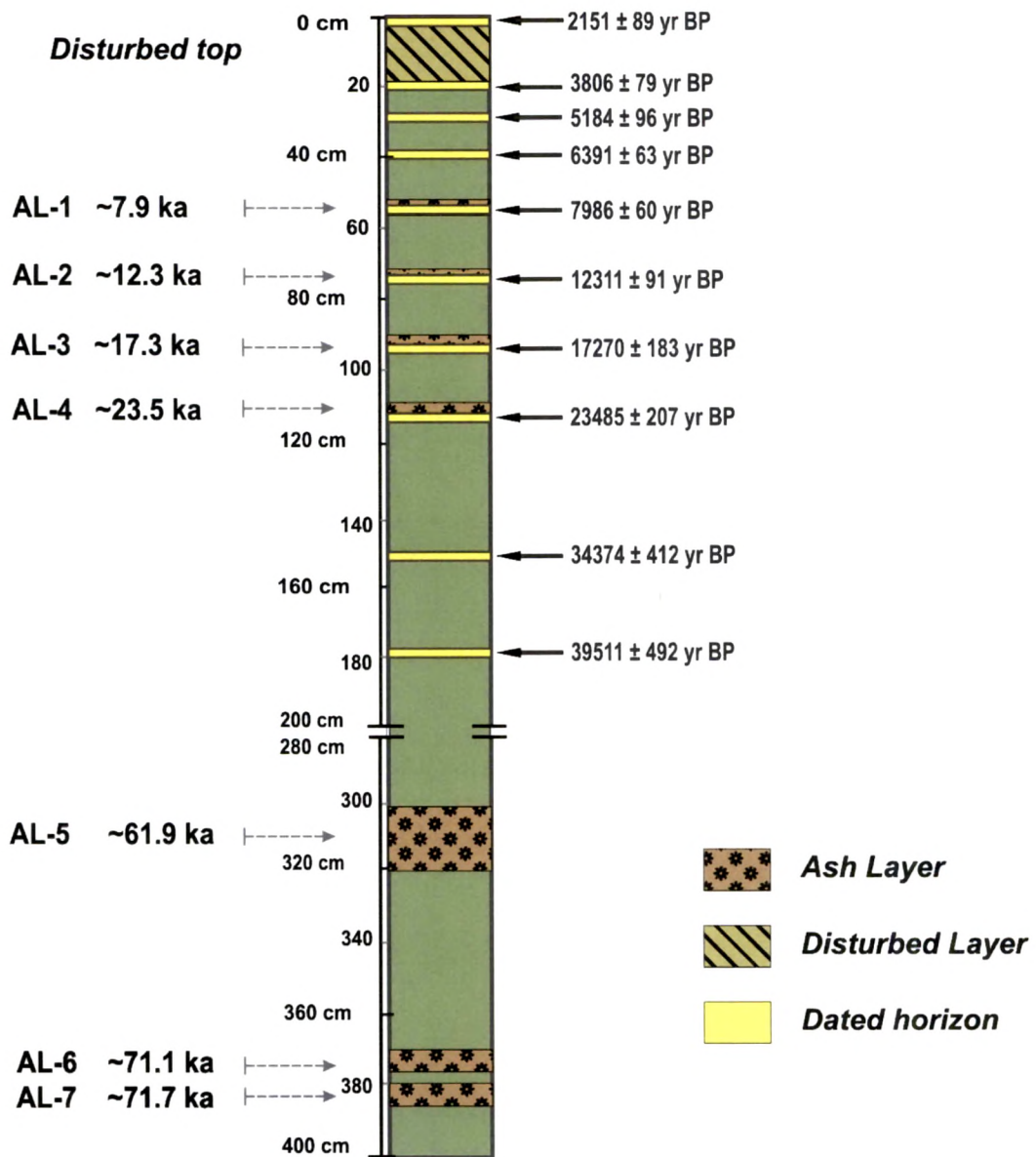


Fig. 3.3: Litholog of core SK-234-60 showing ash layers (AL-1 to 7) with calibrated AMS ¹⁴C ages (in yr BP) for selected sediment layers and estimated ages of the ash layers on the left.

Assuming that the rates of sedimentation had also remained constant within the dated intervals, the ages of the ash layers were estimated (Fig. 3.4). Due to the limitation of

the radiocarbon technique the age of ash layers AL-5 through 7 were not determined directly but extrapolated using the sedimentation rate of 5.5 cm/kyr assuming a constant rate of sedimentation below the bottommost dated band (Fig. 3.4). The estimated ages of the ash layers are given in Figs. 3.3 and 3.4. According to the age model, the 4m long-core covers the last ~74 ka. Based on individual rates of sedimentation the average rate for our core is estimated to about 5.3 cm/kyr.

Table 3.1: AMS ^{14}C ages of planktic foraminifera from core SK-234-60

Core depth (cm)	Tephra code	Conventional radiocarbon age ⁽¹⁾ (cal. kyr BP)	Foraminifer Species	AMS age ⁽²⁾ (cal. kyr BP)	Characteristics of fragments ⁽³⁾
53	Ash Layer-1 (AL-1)	10.1 ± 0.1	Globigerinoides ruber, Globigerinoides sacculifer, Globigerinoides quadilobatus, Globigerinoides bulloides, Globigerinoides triloba, Orbulina universa	7.9 ± 0.1	basaltic andesite to andesite-brown, black vesiculated fragments with translucent feldspar, pyroxene, green olivine, and spinel
73	Ash Layer-2 (AL-2)	14.7 ± 0.2	---do---	12.3 ± 0.1	basaltic to andesite- brown, black highly vesiculated fragments with translucent feldspar and green olivine
90	Ash Layer-3 (AL-3)	18.9 ± 0.3	---do---	17.3 ± 0.2	basaltic andesite to andesite-brown, black highly vesiculated fragments with translucent feldspar, pyroxene, and green olivine
109	Ash Layer-4 (AL-4)	23.5 ± 0.3	---do---	23.5 ± 0.2	basaltic andesite to andesite- grey to black highly vesiculated fragments with translucent feldspar, green olivine and titaniferrous magnetite
302	Ash Layer-5 (AL-5)	61 ± 5 (extrapolated)	–	61.9 ± 2.9 (extrapolated)	andesitic- grey to black poorly vesiculated fragments with translucent feldspar, pyroxene, green olivine, amphibole and titaniferrous magnetite
372	Ash Layer-6 (AL-6)	69 ± 7 (extrapolated)	–	71.1 ± 4.1 (extrapolated)	basaltic andesite- brown, black highly vesiculated fragments with translucent feldspar, pyroxene, and green olivine
380	Ash Layer-7 (AL-7)	70 ± 7 (extrapolated)	–	71.7 ± 4.1 (extrapolated)	basaltic andesite- brown, black highly vesiculated fragments with translucent feldspar pyroxene, and green olivine

Superscript (1): Conventional radiocarbon ages were determined on bulk carbonates using liquid scintillation counter and calibrated with the CALIB 6.0 software (Reimer et al., 2009), considering reservoir correction (ΔR) value of 11 ± 35 yrs for the Andaman Sea (Dutta et al. 2001). The last three ash layers were dated by linear extrapolation.

Superscript (2): AMS ^{14}C dating done at monospecific planktic foraminifer species and calibrated with the CALIB 6.0 software (Reimer et al., 2009). The last three ash layers were dated by linear extrapolation. Superscript (3): Petrological characteristics of lithic fragments were determined by EPMA.

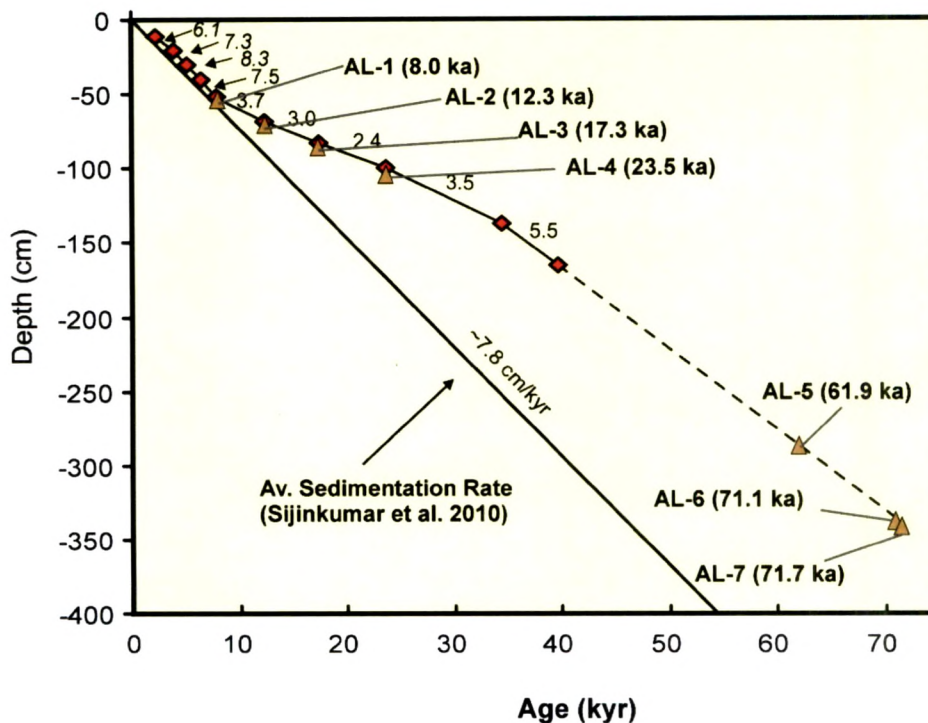


Fig. 3.4: Depth versus age plot for the studied core. Red diamonds represent dated sediment intervals and yellow triangles are ash layers (AL-1 to 7). The numbers on the lines represent sedimentation rates (cm/kyr). Ash layer thicknesses have been removed in sedimentation rate calculation. The dashed line connects the bottommost dated sediment interval to the ash layers 5–7, assuming a constant sedimentation rate of 5.5 cm/kyr- derived from the overlying dated intervals. The straight solid line represents time-averaged sedimentation rate from a nearby core SK-168/GC-1 (Sijinkumar et al., 2010).

Petrographic studies of grains from these ash layers revealed that they were mostly vesiculated lithic fragments that contained microcrystal of translucent plagioclase, black pyroxene, and green olivine (Fig. 3.5, Table 3.1). Chemistry of lithic fragments also confirmed the presence of plagioclase, pyroxene, olivine, titaniferrous magnetite and amphibole embedded in matrix of glass (see Table 3.3). Most of the feldspar grains in lithic fragments show labradorite (An50-70%) and bytownite (An70-85%) compositions (Fig. 3.6a). The grains of AL-6 fall dominantly in the field of bytownite. The pyroxene grains in lithic fragments are mainly augite and (clino) enstatite (Fig. 3.6b). AL-5 contains a few grains of diopside too. Olivines in the ash layers AL-1, 4, 6 show uniform composition with Fo content between 75 and 90%. Hornblende, spinel

and titaniferrous magnetite are found in AL-5, AL-1 and AL-4 & 5, respectively. Spinel of AL-1 have 22-25 wt. % of Cr_2O_3 and while Fe-Ti oxides in AL-4 & 5 have TiO_2 contents up to 9–10 wt. %.

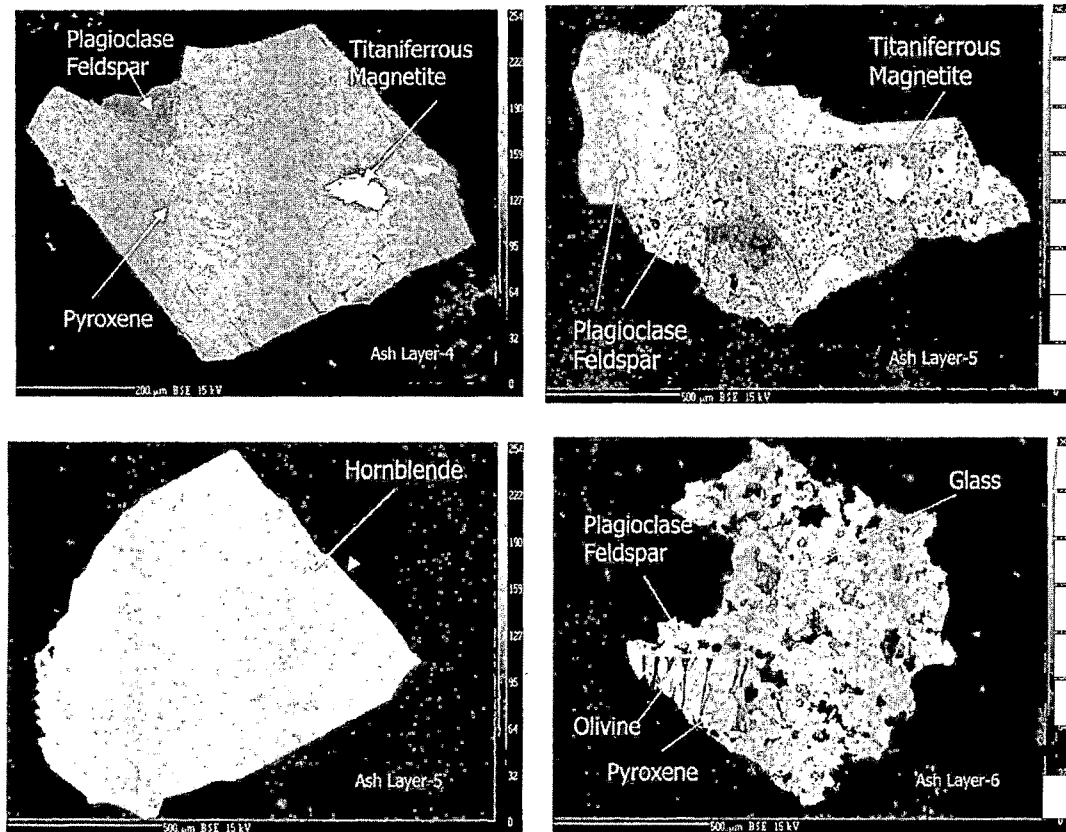


Fig. 3.5: Backscattered X-ray images of lithic fragments and mineral grains from the ash layers of the studied core. Most of the lithic fragments show large and scattered vesicles with thin walls.

3.4.2 Isotope fingerprinting and Origin

To determine the source(s) of these ash layers, we compared Sr and Nd isotopic compositions of core ash layers (AL-1 to 7) with published data for major volcanoes of the Indonesian Arc, Barren Island and Narcondam (Fig. 3.7). The $^{87}\text{Sr}/^{86}\text{Sr}$ and ϵ_{Nd} values of the ash layers in the core vary from 0.70395 to 0.70414, and 6.7 to 4.9, respectively (Table 3.2). These data plot well within the field of lava flows and ash of the Barren Island Volcano (Fig. 3.7), whereas data for ash and lava derived from all other volcanoes of the Indonesian Arc and Narcondam, plot well outside this field. The apparent differences between the isotopic ratios of ash from the core (and lavas of Barren Island) and those of other volcanoes in the Indonesian Arc, despite their

common tectonic settings, are related to the differences in the specific mantle sources and crustal architecture and lithology under each volcano.

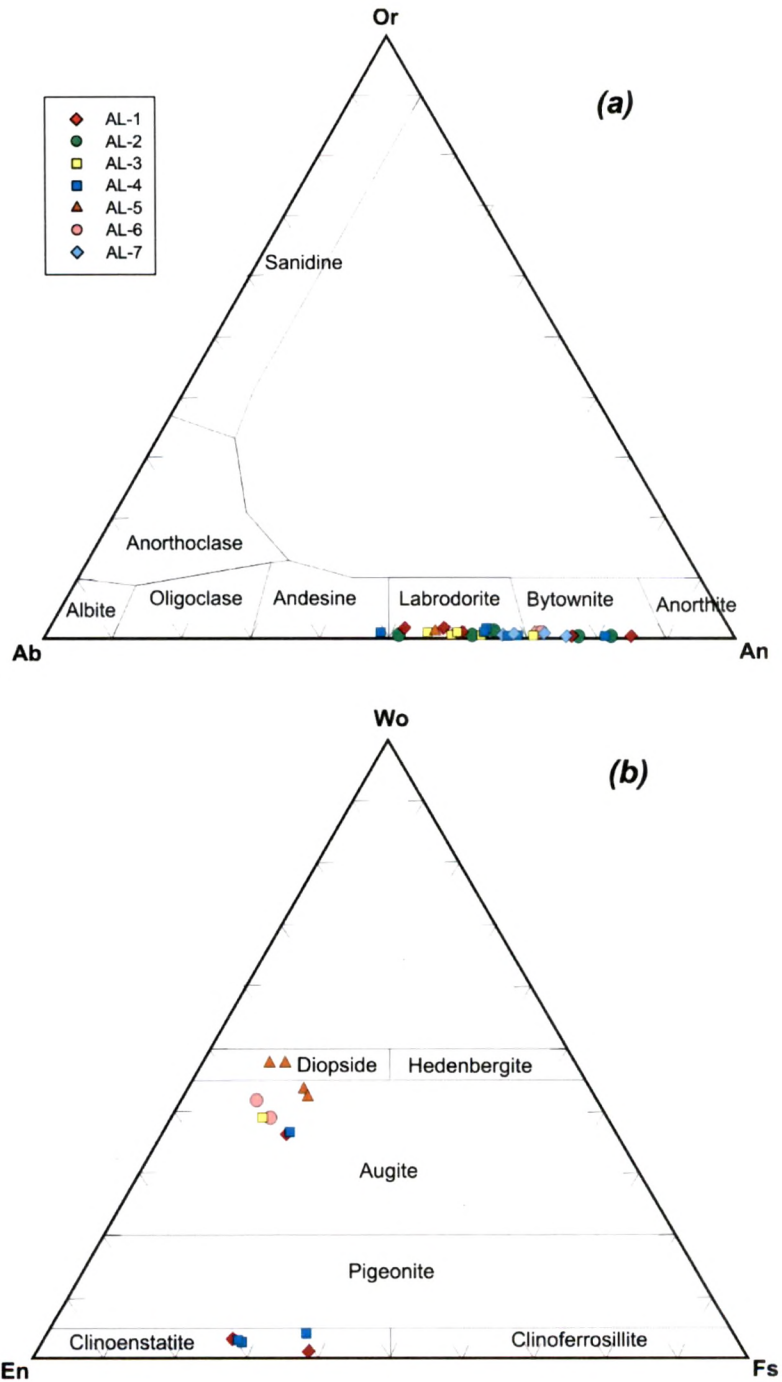


Fig. 3.6: (a) Classification of feldspars found in the ash layers of the core; (b) classification of pyroxene crystals from the core.

These observations clearly establish that the Barren Island Volcano, located 32 km northwest of our core site, as the unique source for the ash layers. Although some values from Rinjani and Galunggung volcanoes overlap with the range observed in our data, we believe that these volcanoes are too far away to have contributed significantly to the core site. None of the ash layers in our core can be correlated with the prominent and widespread ash from the ~74 ka Toba (Sumatra) supereruption (e.g., Pattan et al., 2001 and references therein) and petrographically more evolved (and more highly explosive?) eruptions from other volcanoes of the Indonesian arc.

Table 3.2: Isotopic ratio data for ash layers in the core, ash deposits on Barren Island and lava flows of Narcondam Island.

Sample	Age of Eruption	$^{87}\text{Sr}/^{86}\text{Sr}^a$	$^{143}\text{Nd}/^{144}\text{Nd}^a$	ϵ_{Nd}^b
Ash layers in the core				
	(Estimated - ka) ^c			
AL1 (53-57 cm)	8.0±0.1	0.704	0.512982	6.7
AL2 (23-75 cm)	12.3±0.1	0.70409	0.512891	4.9
AL3 (90-94 cm)	17.3±0.2	0.70409	0.512943	5.9
AL4 (109-112 cm)	23.5±0.2	0.7041	0.512919	5.5
AL5 (302-321 cm)	61.9±2.9	0.70414	0.512938	5.9
AL6 (372-377cm)	71.1±4.1	0.70395	0.512937	5.8
AL7 (380-387cm)	71.7±4.1	0.70401	0.512925	5.6
Ash deposits on Barren				
	(Relative Age)			
BI-07-TL-02	Precaldera	0.704	0.512954	6.2
BI-07-TL-03	Precaldera	0.70393	0.51297	6.5
BI07-TL-06	Precaldera	0.70396	0.512989	6.8
BI-08-TL-01	Precaldera	0.70397	0.512921	5.5
BI-08-TL-02	Precaldera	0.70401	0.512971	6.5
BI-07-TL-05	Unknown	0.70409	0.512928	5.7
BI-07-TL-04	Unknown	0.70404	0.512903	5.2
BI-07-TL-01 (2007)	Modern	0.70413	0.512876	4.6
BI-07-06	Modern	0.70404	0.5129	5.1
BI-09-02 (2009)	Modern	0.70411	0.512872	4.6
Narcondam Island Lava				
NCI-09-09	Unknown	0.70444	0.512754	2.3
NCI-09-19	Unknown	0.70503	0.51271	1.4

Superscript 'a': $^{87}\text{Sr}/^{86}\text{Sr}$ is normalized to 0.71025 for NBS987 and $^{143}\text{Nd}/^{144}\text{Nd}$ is normalized to 0.511858 for LaJolla. Superscript 'b': $\epsilon_{\text{Nd}} = \{ (^{143}\text{Nd}/^{144}\text{Nd})_{\text{sample}} / (^{143}\text{Nd}/^{144}\text{Nd})_{\text{chondrite}} - 1 \} \times 10^4$ and is calculated using an average $(^{143}\text{Nd}/^{144}\text{Nd})_{\text{chondrite}}$ of 0.512638. Superscript 'c' 1 sigma errors, estimated using standard error propagation method, on ages in yrs BP (ka).

The major element oxide data of the lithic fragments from these ash layers also support the inference that ash layers in the core originated from the Barren Island Volcano. In K_2O vs. SiO_2 and TiO_2 vs. Al_2O_3 plots (Fig. 3.8) the data for glass matrix of grains from the ash layers largely overlap with the field of Barren Island. In the core, therefore, it appears that the Barren Island Volcano was the only major eruptive centre in the Andaman Sea during the Late Pleistocene and Holocene and that its debris covered an extensive area around the volcano. Comparing these data with the volcanoclastics preserved in Miocene-Pliocene sedimentary deposits of Andaman Islands and Havelock Island, it was observed that the older ash deposits were completely different in composition and none of these are correlateable to present day volcanoes in the Andaman Sea. The compositions of plagioclase feldspars and pyroxenes in lithic fragments are also similar that reported in samples from Barren Island (Luhr and Halder, 2006; Pal et al., 2010b).

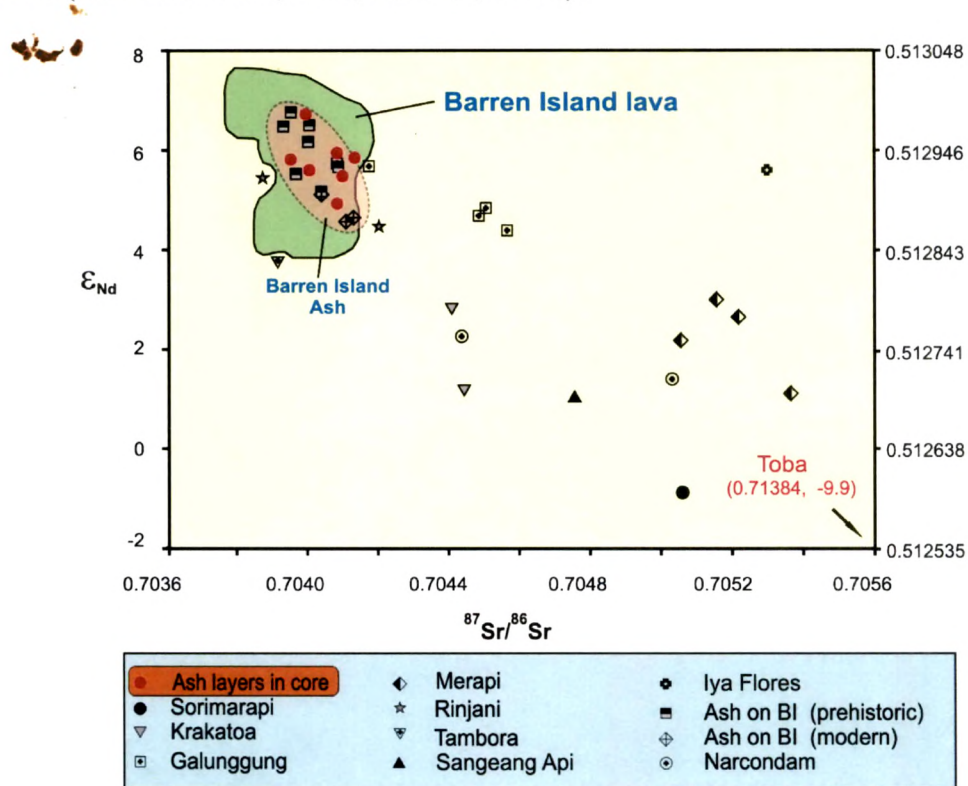


Fig. 3.7: Plot of ϵ_{Nd} versus $^{87}Sr/^{86}Sr$ for the ash layers in the core, ash deposits on Barren Island, and volcanics from some major volcanoes of Indonesia (see Fig. 3.1a). Also shown is a field for isotopic compositions of lava flows on Barren Island. Data sources: Ash layer in the core, ash deposits on Barren Island, and lavas on Narcondam: this work; Barren Island lavas: Luhr and Halder (2006); Chandrashekhram et al. (2009); Kumar (2011); lavas and ash from volcanoes of Indonesia: Turner et al. (2001). All data were normalized to NBS-987 (0.710250) and La Jolla (0.511858) for $^{87}Sr/^{86}Sr$ and $^{143}Nd/^{144}Nd$ isotopic ratios respectively.

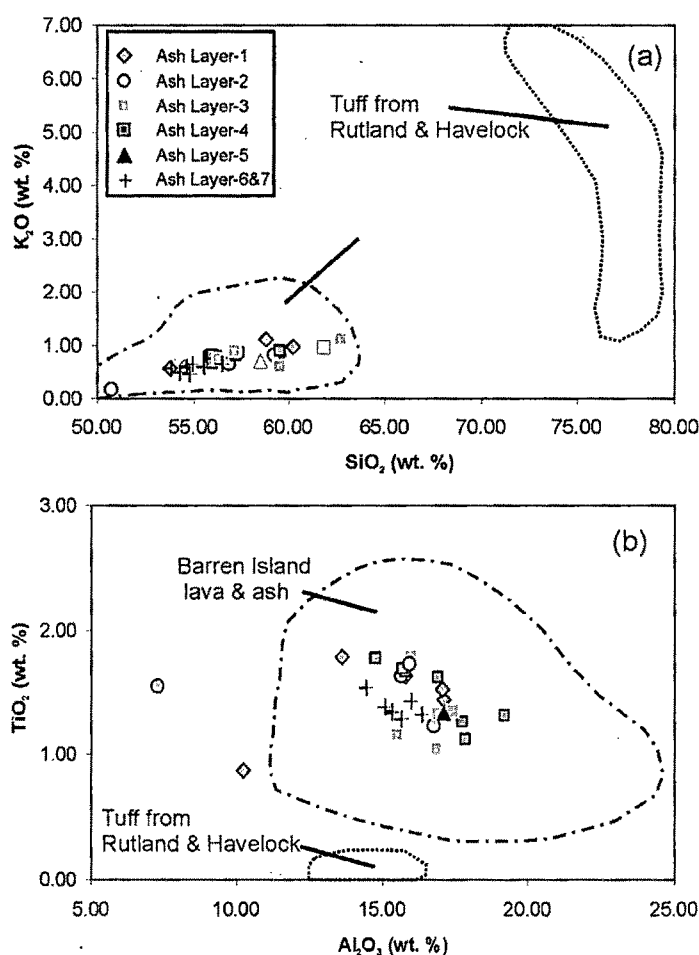


Fig. 3.8: (a) SiO_2 vs. K_2O and (b) Al_2O_3 vs. TiO_2 cross plots showing diagram showing the compositions of the marine ash-layers in the core SK-234-60 compared with the field for the recent volcanics from Barren Island and tuff deposits from Rutland & Havelock. Data source: Barren Island (Kumar, 2011; Luhr and Haldar, 2006; Chandrasekharam et al. 2009; Pal et al., 2010b), Rutland & Havelock (Pal et al., 2005, 2010a).

3.5 History of volcanism on Barren Island

3.5.1 The Barren Island Volcano

The Barren Island Volcano has been described as a stratovolcano, which rises from the depth of more than 2 km of the Andaman seafloor (Sheth et al., 2009a). The exposed part of the volcano represents only the top part of a vastly larger submarine volcano, mostly evolved below sea level. The Barren Island Volcano must have erupted several times in the past but it was only since 1789, the records of its eruptions have been documented. The first recorded eruption occurred during 1789-1832 and after long period of quiescence, the volcano again became active in 1991 (recent) and eruptions are still continuing (Shanker et al., 2001; Luhr and Haldar, 2006; Pal et al., 2007a;

Sheth et al., 2009a, 2010) (Fig. 3.9b). In literature, the undated volcaniclastic deposits and lava flows exposed on the island are mainly divided into pre- and post-caldera volcanic episodes.

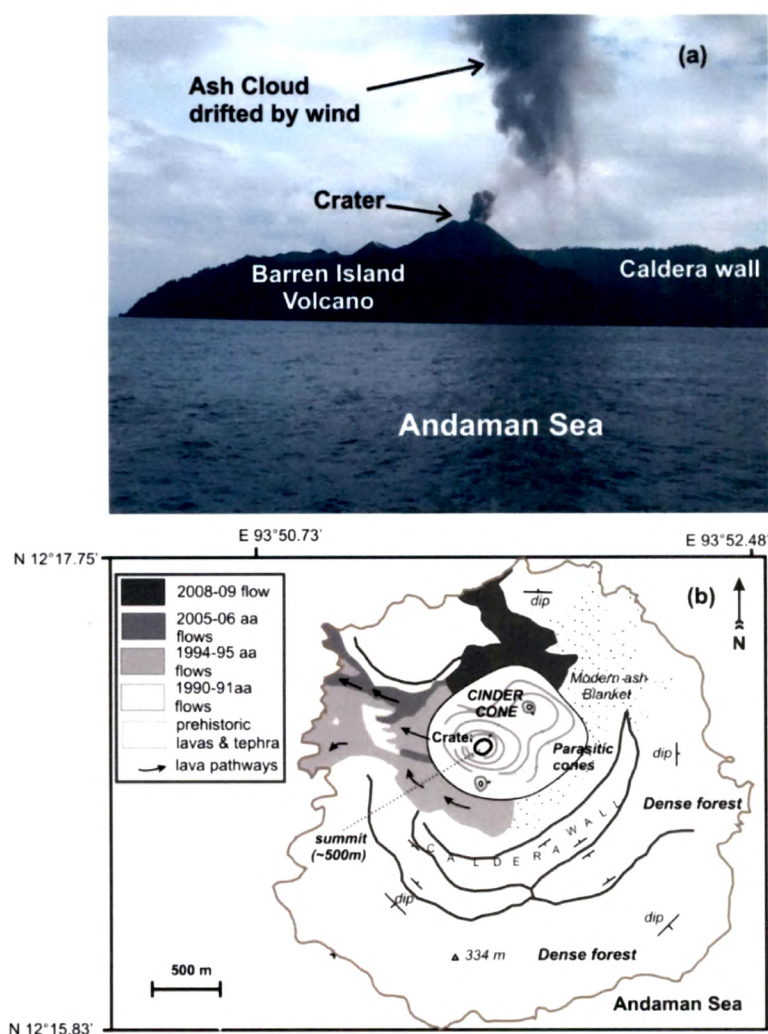


Fig. 3.9: (a) Ash cloud from 2010 eruption of Barren Island Volcano, finer ash is drifted away by the wind and deposited later in the sea nearby (b) Map of Barren Island showing various lava flows and ash distributed from the recent and past eruptions of the volcano.

The volcano has generally shown Strombolian and sometimes Plinian type of eruption. Figure 3.9 (a) shows a recent ash eruption of the volcano, the coarser ash particles show explosive ejection with ballistic trajectories unaffected by the wind while finer ones are drifted away by the wind and get deposited in the nearby sea. Probably ash layers in our core were also deposited in similar fashion. In the Andaman Sea, the predominant wind directions are southwesterly during summer (May-September) and northeasterly during

winter (October-April). These winds should promote dispersal mainly into the northeast and southwest part of the sea from the volcano. Our core location is in the southeast of the volcano. We, therefore, believe that the ashes deposited in our core were transported by surface currents from near the volcano and not by direct aerial dispersal, and likely represent major eruptions.

Our core recorded at least seven major eruptions of the volcano during the last ~74 kyr. Presence of the two distinct ash layers near the bottom of the core, with irresolvable ages due to high errors on the estimates, suggests a couple of major eruptions of the volcano at ~71 ka. Another major eruption is recorded at ~62 ka. Interestingly, the ~62 ka ash layer (AL-5) is the thickest in the entire record and contains the coarsest of volcanic grains (~2 mm) in the core. This suggests that the intensity of the ~62 ka eruption was quite large, and we speculate that this was the time the volcano had grown to near sea level or above it. Absence of any ash layer between AL-5 (302 cm, ~62 ka) and AL-4 (112 cm, ~24 ka) points to a significant hiatus between these large ash eruptions (Fig. 3.3). Since the eruption at ~24 ka, the volcano has had fairly regular major eruptions every ~5000 years until the ~8 ka eruption.

The variation of ϵ_{Nd} value of the ash layers of the core (Table 3.2) between the ~71 ka and the ~17 ka eruptions is very small (marginally higher than the analytical 2σ uncertainty of 0.2 units), which indicates that the Nd isotopic composition of magma of the Barren Island remained almost constant during this large time period. This is significant for the large time interval represented. The first marked change in magma composition is observed in the ~12 ka eruption, and since then the composition has been variable as is apparent from the variable ϵ_{Nd} of historic and recent eruptions on Barren Island (Table 3.2; Luhr and Haldar 2006; Chandrasekharam et al. 2009). The highest ϵ_{Nd} value measured for ash layers of the core is 6.7, a composition shown only by the lavas and ash deposits of the Barren Island that are exposed in the caldera wall of the volcano ($\epsilon_{Nd} > 6.0$), and which thus predate the caldera itself. In comparison, all historic and modern (caldera-filling) eruptions of the volcano have produced lava and ash with much lower ϵ_{Nd} values (~5.0 or less) (Table 3.2; Luhr and Haldar 2006;

Table 3.3: Major element oxide contents (in wt %) of Plagioclase feldspar; pyroxene; olivine; titaniferrous magnetite, amphibole and spinel in the ash layers of the core SK-234-60

	SiO ₂	TiO ₂	Al ₂ O ₃	FeO	MnO	MgO	CaO	Na ₂ O	K ₂ O	P ₂ O ₅	Cr ₂ O ₃	CoO	NiO
<i>Feldspar</i>													
AL-1													
LF-1	46.16	0.04	33.61	0.76	0.02	0.12	17.31	1.68	0.03	0.24		0.03	Bytownite
LF-2	48.44	0.07	31.52	1.19	0.01	0.41	15.52	2.56	0.07	0.19		0.01	Bytownite
LF-3	55.66	0.43	25.25	2.66	0.04	0.40	10.03	5.00	0.31	0.18		0.05	Labradorite
LF-4	53.30	0.74	24.39	4.77	0.03	0.88	10.93	4.35	0.30	0.22	0.02	0.02	Labradorite
LF-5	53.23	0.10	28.07	1.34	0.05	0.31	12.21	4.31	0.16	0.16	0.02	0.01	Labradorite
LF-6	52.34	0.09	29.17	0.92	0.05	0.11	12.55	4.46	0.08	0.16	0.03	0.03	Labradorite
AL-2													
LF-1	49.68	0.08	30.85	1.03	0.01	0.11	14.72	3.16	0.06	0.19	0.01	0.06	Bytownite
LF-3	51.26	0.06	29.58	0.91	0.01	0.21	13.51	4.09	0.16	0.15	0.02	0.01	Labradorite
LF-4	51.95	0.07	29.42	0.92	0.02	0.13	12.99	4.22	0.07	0.15	0.02	0.01	Labradorite
LF-5	46.93	0.02	33.14	0.72	0.00	0.06	16.80	2.03	0.03	0.20	0.01	0.03	Bytownite
LF-6	54.65	0.08	27.52	0.98	0.04	0.14	10.81	5.52	0.09	0.09		0.07	Labradorite
LF-7	48.01	0.03	32.35	0.57	0.02	0.04	16.17	2.50	0.06	0.19	0.01	0.01	Bytownite
AL-3													
LF-1	52.09	0.13	28.95	1.27	0.02	0.19	12.82	4.21	0.10	0.17	0.01	0.03	Labradorite
LF-2	53.00	0.15	28.39	1.27	0.04	0.15	12.13	4.56	0.12	0.16	0.01	0.02	Labradorite
LF-3	51.36	0.08	29.31	1.26	0.01	0.15	13.34	4.16	0.07	0.17	0.02	0.04	Labradorite
LF-4	53.04	0.24	27.58	1.85	0.05	0.34	12.05	4.42	0.17	0.18	0.02	0.03	Labradorite
LF-5	50.28	0.05	30.46	0.97	0.03	0.12	14.25	3.54	0.08	0.17	0.02	0.01	Labradorite
LF-6	49.80	0.06	30.64	1.00	0.01	0.11	14.81	3.29	0.06	0.18		0.02	Bytownite
LF-7	53.86	0.16	27.50	1.60	0.02	0.23	11.38	4.91	0.14	0.16	0.03	0.00	Labradorite
AL-4													
LF-2	47.45	0.03	32.47	0.87	0.06	0.16	16.72	2.05	0.03	0.20			Bytownite
LF-3	50.33	0.03	30.92	0.80	0.08	0.06	13.85	3.62	0.05	0.18		0.08	Labradorite
LF-4	50.73	0.09	30.05	1.25	0.03	0.16	13.95	3.46	0.09	0.18	0.02	0.02	Bytownite
LF-5	52.13	0.25	29.21	1.87	0.03	0.34	12.04	3.63	0.27	0.21	0.02	0.03	Labradorite
LF-6	55.72	0.24	28.42	1.60	0.02	0.21	8.55	4.85	0.14	0.19	0.02	0.01	Andesine
LF-7	52.23	0.26	27.86	2.18	0.01	0.43	12.74	3.92	0.18	0.16	0.03	0.01	Labradorite
AL-5													
LF-1	54.70	0.04	28.00	0.56	0.04	0.06	11.44	4.70	0.22	0.19	0.01	0.01	Labradorite
LF-2	49.95	0.03	30.93	0.60	0.05	0.10	14.81	3.24	0.07	0.14	0.02	0.03	Bytownite
LF-5	46.85	0.03	33.17	0.62	0.04	0.06	17.10	1.84	0.03	0.20	0.01	0.01	Bytownite
LF-7	51.92	0.30	27.76	2.26	0.07	0.47	13.02	3.75	0.26	0.15	0.02	0.01	Labradorite

Table 3.3: Continued

	SiO ₂	TiO ₂	Al ₂ O ₃	FeO	MnO	MgO	CaO	Na ₂ O	K ₂ O	P ₂ O ₅	Cr ₂ O ₃	CoO	NiO	
AL-6														
LF-1	49.95	0.16	30.01	1.60	0.02	0.59	14.25	3.04	0.10	0.20	0.02	0.03	0.02	Bytownite
LF-2	49.73	0.19	29.82	1.87	0.03	0.47	14.51	3.00	0.11	0.23	0.01	0.02	0.01	Bytownite
LF-3	48.68	0.07	31.43	1.03	0.04	0.19	15.59	2.66	0.06	0.20	0.03	0.01	0.01	Bytownite
AL-7														
LF-4	50.66	0.05	30.89	0.70	0.01	0.15	13.69	3.50	0.05	0.18	0.01	0.00	0.09	Labradorite
LF-5	51.08	0.04	30.73	0.76	0.13	0.13	13.25	3.70	0.06	0.19	0.02	0.03	0.01	Labradorite
LF-6	49.81	0.15	30.63	1.55	0.03	0.44	14.10	2.91	0.07	0.20	0.04	0.04	0.02	Bytownite
LF-7	48.91	0.07	32.05	1.10	0.04	0.19	14.79	2.53	0.06	0.22	0.01	0.01	0.03	Bytownite
Pyroxene														
AL-1														
LF-2	59.18	0.07	3.31	18.70	0.04	16.84	0.49	0.25	0.98	0.04		0.01	0.11	Clinoenstatite
LF-5	50.83	0.78	2.86	11.10	0.35	15.38	18.03	0.28	0.01	0.21	0.12	0.01	0.03	Augite
LF-7	53.60	0.33	1.43	16.90	0.49	25.49	1.65	0.03	0.00	0.02	0.01	0.02	0.02	Clinoenstatite
AL-3														
LF-5	51.40	0.55	2.27	8.62	0.26	16.66	19.18	0.33	0.01	0.26	0.35		0.11	Augite
AL-4														
LF-1	54.22	0.33	1.31	17.41	0.47	25.09	1.55	0.03	0.02	0.01			0.02	Clinoenstatite
LF-2	52.05	0.58	3.00	10.70	0.30	15.65	17.30	0.41	0.01	0.18			0.11	Augite
LF-3	53.34	0.23	1.24	17.79	0.68	25.18	1.42	0.04	0.01	0.02	0.02	0.03	0.01	Clinoenstatite
LF-6	45.69	0.35	8.88	20.78	0.36	19.16	1.89	2.39	0.19	0.26		0.05		Augite
AL-5														
LF-1	51.78	0.41	1.52	10.59	0.37	13.95	20.78	0.35		0.21	0.04			Augite
LF-3	49.58	0.74	4.57	7.38	0.12	13.98	23.01	0.26	0.01	0.25	0.05	0.03	0.03	Diopside
LF-4	51.73	0.36	1.40	9.92	0.53	14.05	21.40	0.31	0.01	0.23	0.03	0.01	0.02	Augite
LF-7	50.84	0.51	3.50	5.93	0.14	14.88	23.22	0.23		0.25	0.47		0.04	Diopside
AL-6														
LF-1	52.39	0.49	2.51	7.89	0.23	16.60	18.85	0.32	0.02	0.25	0.38	0.05		Augite
LF-2	51.89	0.52	3.43	6.60	0.12	16.34	20.06	0.22	0.01	0.25	0.47	0.02	0.09	Augite
Olivine														
AL-1														
LF-4	38.06	0.01	0.10	20.90	0.31	40.22	0.20	0.01	0.01	0.03	0.03		0.10	Chrysolite
AL-4														
LF-2	39.29	0.01	0.07	18.70	0.33	41.53	0.28					0.09	0.01	Chrysolite
LF-6	39.00	0.03	0.51	22.31	0.39	37.14	0.25	0.08	0.01	0.13	0.08	0.08	0.01	Chrysolite

Table 3.3: Continued

	SiO ₂	TiO ₂	Al ₂ O ₃	FeO	MnO	MgO	CaO	Na ₂ O	K ₂ O	P ₂ O ₅	Cr ₂ O ₃	CoO	NiO	
LF-7	39.98	0.02	0.29	17.64	0.22	41.72	0.21	0.01	0.01	0.01		0.11		Chrysolite
<i>AL-6</i>														
LF-1	40.44	0.01	0.03	10.83	0.15	47.91	0.19	0.02		0.01	0.04	0.05	0.32	Chrysolite
LF-3	38.98	0.02	0.05	18.52	0.31	41.65	0.25	0.02	0.01	0.02	0.02		0.16	Chrysolite
LF-4	39.62	0.02	0.12	17.21	0.41	42.07	0.25	0.03		0.03	0.07		0.16	Chrysolite
LF-5	38.82	0.02	0.05	20.99	0.37	39.35	0.17	0.07		0.01	0.02	0.02	0.13	Chrysolite
LF-6	39.90	0.01	0.06	15.85	0.26	43.36	0.20	0.09			0.07	0.01	0.18	Chrysolite
<i>Titaniferous Magnetite</i>														
<i>AL-4</i>														
LF-3	2.34	10.18	4.64	78.08	0.54	3.73	0.17	0.22	0.02		0.04	0.03	0.02	
<i>AL-5</i>														
LF-2	0.56	8.85	1.96	86.57	0.77	1.21	0.04			0.69	0.03	0.00	0.01	
LF-4	0.24	9.41	2.42	83.68	0.71	1.72	1.04	0.04			0.04			
<i>Amphibole</i>														
<i>AL-5</i>														
LF-6	42.50	2.28	13.41	11.95	0.11	14.68	12.20	2.49	0.18	0.14	0.02	0.02	0.02	Ferroan Pargasite
<i>Spinel</i>														
<i>AL-1</i>														
LF-4	0.18	3.12	11.89	53.24		6.69	0.08	0.02			24.65		0.13	Cr-Spinel

*Values are normalised to a total of 100 wt. %. AL: Ash Layer; LF: Lithic Fragment. Minerals are classified on the basis of their chemical compositions using software Minpet 2.02 (Richard, 1995).

Table 3.4: Major element oxide contents (in wt %) of glass matrix in the ash layers of the core SK-234-60

	SiO ₂	TiO ₂	Al ₂ O ₃	FeO	MnO	MgO	CaO	Na ₂ O	K ₂ O	P ₂ O ₅	Cr ₂ O ₃	CoO	NiO	Mg#	FeO/(MgO)
AL-1															
LF-2	54.49	1.78	13.63	14.35	0.17	8.34	4.64	1.80	0.59	0.16	0.01	0.01	0.02	50.86	1.72
LF-3	60.17	1.63	15.82	8.66	0.21	2.26	6.11	3.83	0.97	0.31	0.01	0.02	0.01	31.75	3.83
LF-4	53.80	1.44	17.11	9.06	0.23	3.51	10.18	3.79	0.57	0.24	0.03	0.01	0.03	40.85	2.58
LF-5	58.77	0.87	10.22	9.37	0.17	6.68	10.42	1.99	1.12	0.32	0.06	0.01		55.96	1.40
LF-6	59.49	1.53	17.09	7.83	0.18	1.64	6.32	4.74	0.82	0.30	0.02	0.03	0.04	27.18	4.77
AL-2															
LF-1	56.32	1.72	15.97	10.00	0.21	2.67	8.15	3.86	0.75	0.30	0.01	0.02	0.04	32.24	3.74
LF-2	56.85	1.23	16.79	9.19	0.23	3.19	7.77	3.84	0.64	0.21	0.02	0.01	0.03	38.20	2.88
LF-4	50.72	1.54	7.29	11.70	0.41	10.42	16.10	1.37	0.17	0.27	0.02			61.35	1.12
LF-6	59.23	1.63	15.66	9.06	0.22	2.62	6.66	3.73	0.81	0.31	0.02	0.04	0.03	34.01	3.46
AL-3															
LF-1	56.19	1.69	15.72	10.00	0.22	3.24	7.89	3.88	0.78	0.30	0.02	0.04	0.04	36.59	3.09
LF-2	57.41	1.66	15.81	9.24	0.24	2.50	7.68	4.21	0.86	0.33	0.02	0.01	0.01	32.53	3.70
LF-3	55.84	1.61	16.96	9.60	0.21	2.64	8.19	3.81	0.79	0.28	0.02	0.02	0.03	32.88	3.64
LF-4	57.23	1.26	17.77	7.86	0.20	2.52	7.54	4.46	0.81	0.28	0.02	0.04	0.02	36.36	3.12
LF-5	59.56	1.12	17.85	6.53	0.05	1.78	7.19	4.73	0.89	0.31		0.01		32.68	3.67
LF-6	55.98	1.77	14.79	11.16	0.25	3.51	7.61	3.75	0.82	0.32	0.01	0.02	0.02	35.92	3.18
LF-7	55.97	1.31	19.20	7.62	0.16	1.93	8.42	4.46	0.64	0.26	0.01	0.01	0.01	31.06	3.95
AL-4															
LF-1	61.85	1.04	16.88	6.83	0.19	1.95	5.17	5.00	0.94	0.28	0.03	0.02	0.01	33.72	3.50
LF-2	56.33	1.35	17.46	8.22	0.14	2.43	8.87	4.31	0.72	0.22	0.02	0.06	0.01	34.51	3.38
LF-5	62.70	1.16	15.52	7.65	0.10	2.54	4.73	4.23	1.11	0.31	0.02	0.02	0.01	37.14	3.02
LF-6	59.51	1.33	16.95	8.82	0.19	2.23	5.79	4.16	0.60	0.33	0.02	0.06	0.02	31.05	3.96
LF-7	57.15	1.79	16.02	10.10	0.11	2.38	7.69	3.67	0.88	0.28	0.01	0.03	0.01	29.60	4.24
AL-5															
LF-7	58.46	1.33	17.12	8.02	0.09	2.47	7.64	3.88	0.72	0.22	0.01	0.01	0.02	35.40	3.25
AL-6															
LF-1	54.66	1.32	16.37	9.43	0.19	4.03	9.31	3.79	0.58	0.25	0.03	0.01	0.02	43.22	2.34
LF-2	53.85	1.34	15.35	10.36	0.22	5.41	9.21	3.34	0.57	0.25	0.02	0.00	0.05	48.21	1.91
LF-3	54.97	1.42	15.99	9.90	0.22	3.80	9.18	3.54	0.65	0.27	0.02	0.00	0.02	40.65	2.60
AL-7															
LF-4	56.48	1.53	14.46	10.85	0.26	4.44	7.63	3.38	0.65	0.27	0.02	0.02		42.16	2.44
LF-5	55.53	1.38	15.13	9.82	0.22	4.39	8.80	3.79	0.59	0.27	0.05	0.02	0.03	44.34	2.24
LF-6	54.32	1.29	15.66	10.01	0.16	5.51	8.73	3.42	0.50	0.27	0.05	0.03	0.05	49.52	1.82
LF-7	54.84	1.34	15.34	9.88	0.23	5.07	9.44	3.06	0.45	0.28	0.04	0.01	0.02	47.75	1.95

*Values are normalised to a total of 100 wt. %. AL: Ash Layer; LF: Lithic Fragment.

Chandrasekharam et al., 2009). This relationship may be an indication that the caldera of the Barren Island volcano is younger than ~8 ka, the age of the youngest ash layer in the core with the ϵ_{Nd} value of 6.7. Absence of an identifiable ash layer younger than ~8 ka is well in accord with the hypothesis that the caldera of Barren Island formed as a result of a single, simple, symmetric collapse along circular (ring) faults (Sheth et al., 2009a), and was not associated with a major eruption as speculated by Shanker et al. (2001). Unlike ϵ_{Nd} values, $^{87}Sr/^{86}Sr$ ratios of ash layers in the core overlap with each other, and with that of the ash and lavas on Barren Island (Table 3.2; Luhr and Haldar 2006; Chandrasekharam et al. 2009), and therefore, are of little use as stratigraphic markers. Also, $^{87}Sr/^{86}Sr$ ratio is susceptible to alteration by sea water. Although an attempt has been made here to reconstruct the evolutionary history of the Barren Island Volcano, we acknowledge the fact that data from a single core may not be sufficient to reconstruct the complete eruption history of the volcano, since it is quite possible that many of the past ash eruptions of the volcano were simply not recorded at our core site because of their dispersal in other directions.

3.5.2 Geochemistry of Ash Layers and evolution of the Barren Island Volcano

Major element compositions of glass matrix of the lithic fragments from the ash layers of the core determined using EPMA, are presented in Table 3.4. Based on Total Alkalis-Silica (TAS) classification of volcanic rocks (Fig. 3.10) we determine these fragments to represent sub-alkalic volcanic magma and basaltic to andesitic composition. The majority of these fragments show basaltic to andesitic composition similar to what is observed for most subaerial lava flows on the volcano. This result not only confirms that the all ash layers are generated by the Barren Island Volcano but also suggests that the parental magmas during various eruptions in the past were more evolved than the modern flows (Fig. 3.10).

From the major oxide data it is apparent that the ash in a given layer represents an evolving magma during that particular volcanic event, as various oxide contents in the glass matrix show fractional crystallization trends in plots against MgO content (Fig. 3.11). Mg# (=

[atomic $\text{Mg}/(\text{Mg} + \text{Fe}^{2+}) \times 100$] in a given layer is highly variable (Table 3.4), which suggests that the lithic fragments were erupted at various times during an eruption, when the magma was continuously evolving due to fractional crystallization. Decrease in CaO , FeO^{T} , $\text{CaO}/\text{Al}_2\text{O}_3$ and increase in SiO_2 , Al_2O_3 with decreasing MgO (Fig. 3.11) in glass matrices are indicative of plagioclase and pyroxene fractionation from the magma before it got quenched due to its sudden separation and violent ejection out of the magma chamber. Similar inferences can also be made about fractionation of other minerals from the magma (e.g. titanomagnetite) prior to their removal of the liquid with which it was in equilibrium, as ash grains.

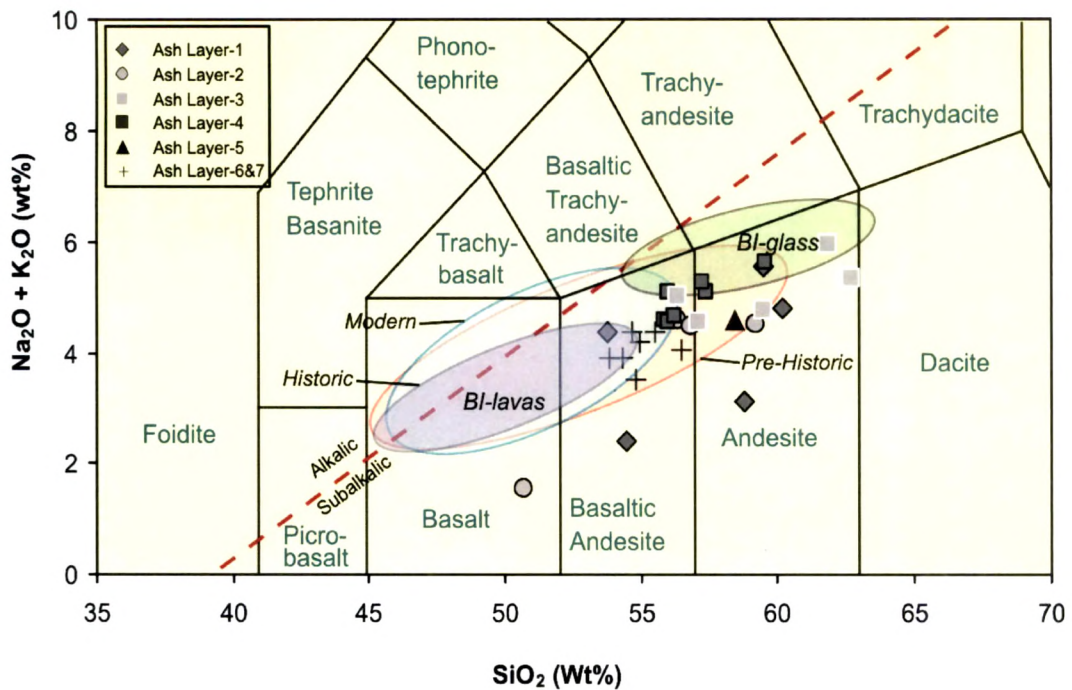


Fig. 3.10: Total Alkalis-Silica (TAS) classification (Le Bas et al., 1986) for glass matrix from lithic fragments for ash layers in the core SK-234-60. For comparison the field for volcanics from Barren Island is also shown. Data sources: Barren Island (Luhr and Haldar, 2006; Chandrasekharam et al., 2009; Pal et al., 2007a, 2010b; Kumar, 2011). The boundary between the alkalic and subalkalic rocks is after Macdonald and Katsura (1964).

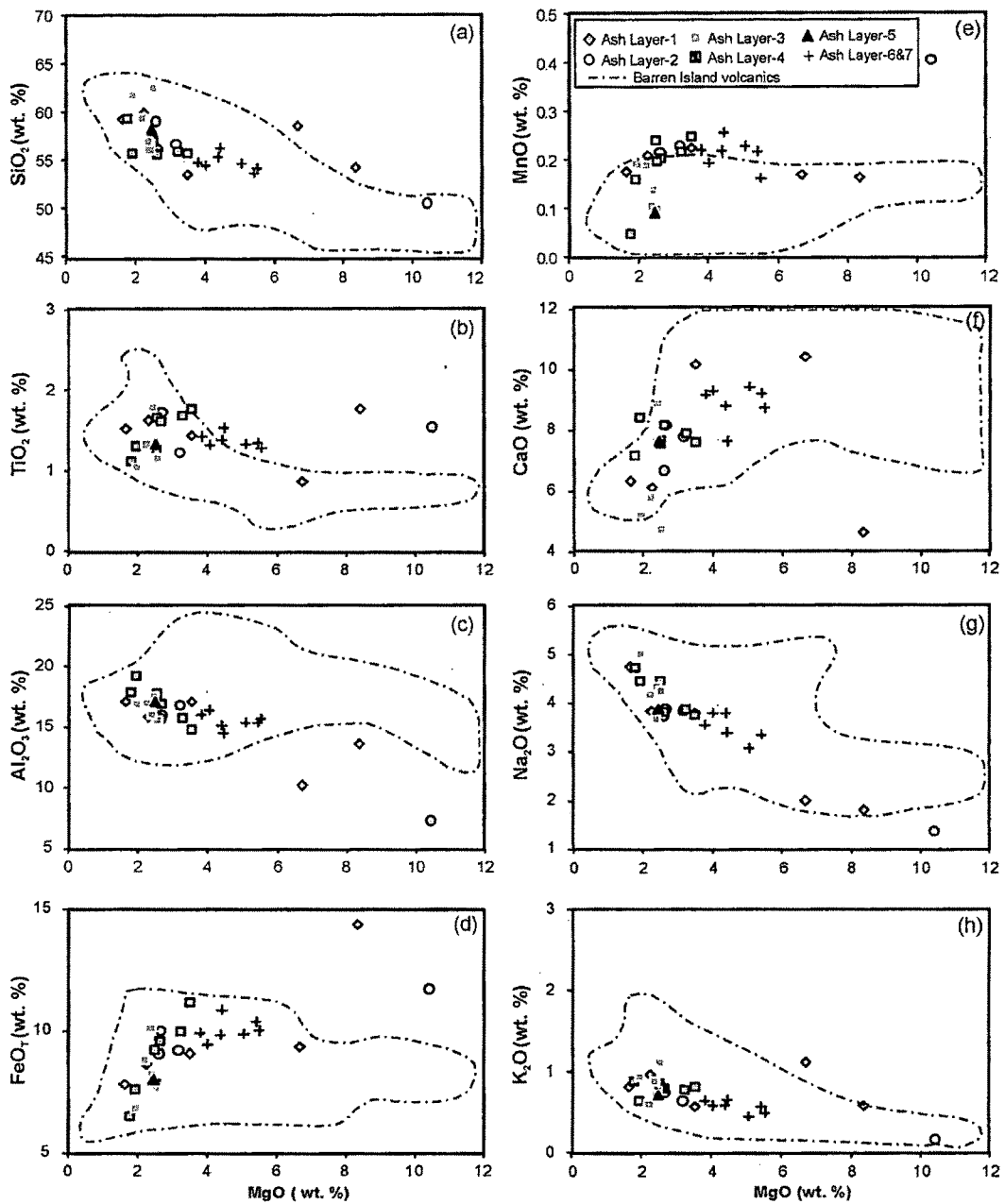


Fig. 3.11: Various major element oxides vs. MgO plots for glass matrix of lithic fragments from the ash layers in the core SK-234-60 compared with field for Barren Island volcanic. Data sources: (Kumar, 2011; Luhr and Haldar, 2006; Chandrasekharam et al., 2009; Pal et al., 2010b).